



Soft Robotics

How to cite: Angew. Chem. Int. Ed. 2025, e18011 doi.org/10.1002/anie.202518011

Dynamic Bonding Enabled Ambient-Driven Motors

Muqing Si⁺, Zixiao Liu⁺, Chi Chen⁺, Wei Lu,* Depeng Liu, Pengju Shi, Yi Yu, Yichen Yan, Ximin He.* and Tao Chen*

Abstract: Harnessing ambient low-density energy and converting it into macroscopic motion is a hallmark of living systems. However, artificial systems are often limited by high energy requirements and intricate control mechanisms. Inspired by Salmonella, which uses dynamic ion-binding coordination for continuous motion, we proposed a novel concept of self-oscillating motors leveraging molecular-level dynamic bonding to harvest trivial ambient energy and power macroscopic, self-sustained behavior. Specifically, we developed a coordination motorized oscillator (CoMO) based on novel supramolecular PDMS material with 25-fold thermo-inflation ability of normal PDMS and nearly 2000-fold that of the passive layer. CoMO can harvest ambient energy as low as body temperature to reversibly dissociate coordination crosslinks, transforming molecular transitions into sustained macroscopic oscillation. Its universality facilitates the amplification of macroscopic motion via the collective behaviors of CoMOs. Moreover, this principle empowers the development of ambient-driven coordination motored robots (CoMbot) with multi-modal locomotion and adaptability across diverse terrains. Such dynamic chemical transitions enabled chemo-mechanical coupling for self-sustained systems, paving new avenues for robust transition-mechanical transducing material systems and soft machineries with unprecedented capabilities.

Introduction

Natural organism serves as masters for inspiring the development of synthetic materials that replicate their dynamic and adaptive behavior^[1–5] The development of such systems has relied on active materials, especially stimuliresponsive polymers, which exhibit reversible property changes (e.g., volume, shape, and stiffness) in response to ambient energy/stimuli fluctuation.^[6–10] The major methods to achieve a repeated response of such material can be concluded as "equilibrium" and "out-of-equilibrium" approaches. The "equilibrium approach" usually relies on cyclic on/off switching or level-changing of external stimuli for the repetitive changing of stimuli-responsive polymers between environmental-corresponding equilibrium

ity/temperature switching [18,19]) are neither feasible nor realistic in actual environments. In contrast, the out-ofequilibrium approach involves the stimuli-material feedback loop (e.g., self-shadowing effect), which makes the state of material waving around the environment-corresponding equilibrium state, to achieve a cyclic response of the material under constant energy input.[20,21] Such cyclic response is quite similar to that of natural organisms, but high-density energy input or concentrated stimulus sources far exceeding ambient conditions (e.g., lasers, [22] heaters, [8,23,24] and humid sources) are required to trigger and sustain such out-ofequilibrium behaviour in artificial systems. These stringent requirements often lead to practical limitations, including interfacial delamination, rapid material degradation, or saturation of the applied stimulus, [25-32] which compromise stability and durability. Such critical requirements also pose challenges to effectively operating such systems and producing bio-like consecutive work output in natural low-energy density environments, restricting the generation of bio-like consecutive work output.^[33-36] For example, photothermalactuated liquid crystal elastomer (LCE) oscillators may delaminate rapidly under continuous laser irradiation.[22,37] Humidity-driven oscillations rely on moisture transport in and out of the material, which is a diffusion-controlled process that inherently limits actuation speed and risks rapid moist saturation of the polymer when it is positioned close to a humid source.[19,38] Similarly, while heat gradients have been explored to drive oscillation in artificial systems, the required temperature thresholds for sustainable operation are often

well above typical environmental conditions, making them

unsuitable for harvesting ubiquitous low-grade energy. [23,39,40]

states.[11-15] However, such deliberately designed varying

surroundings (e.g., large PH variation, [16,17] great humid-

[*] M. Si⁺, W. Lu, D. Liu, Y. Yu, T. Chen State Key Laboratory of Advanced Marine Materials, Zhejiang Key Laboratory of Extreme-environmental Material Surfaces and Interfaces, Ningbo Institute of Materials Technology and Engineering, Chinese Academy of Sciences, Ningbo 315201, China E-mail: luwei@nimte.ac.cn

tao.chen@nimte.ac.cn

M. Si⁺, Z. Liu⁺, C. Chen⁺, P. Shi, Y. Yan, X. He Department of Materials Science and Engineering, University of California, Los Angeles, Los Angeles 90095, USA E-mail: ximinhe@ucla.edu

M. Si⁺, W. Lu, D. Liu, Y. Yu, T. Chen School of Chemical Sciences, University of Chinese Academy of Sciences, Beijing 100049, China

[⁺] These authors contributed equally to this work.

Additional supporting information can be found online in the Supporting Information section

15213773, 0, Downloaded from https

2/onlinelibrary.wiley.com/doi/10.1002/anie.202518011 by University Of California, Los Angeles, Wiley Online Library on [06/11/2025]. See the Terms and Conditions (https://onlinelibrary.wiley.com/terms-and-conditions) on Wiley Online Library for rules of use; OA articles are governed by the applicable Creative Commons Licensea

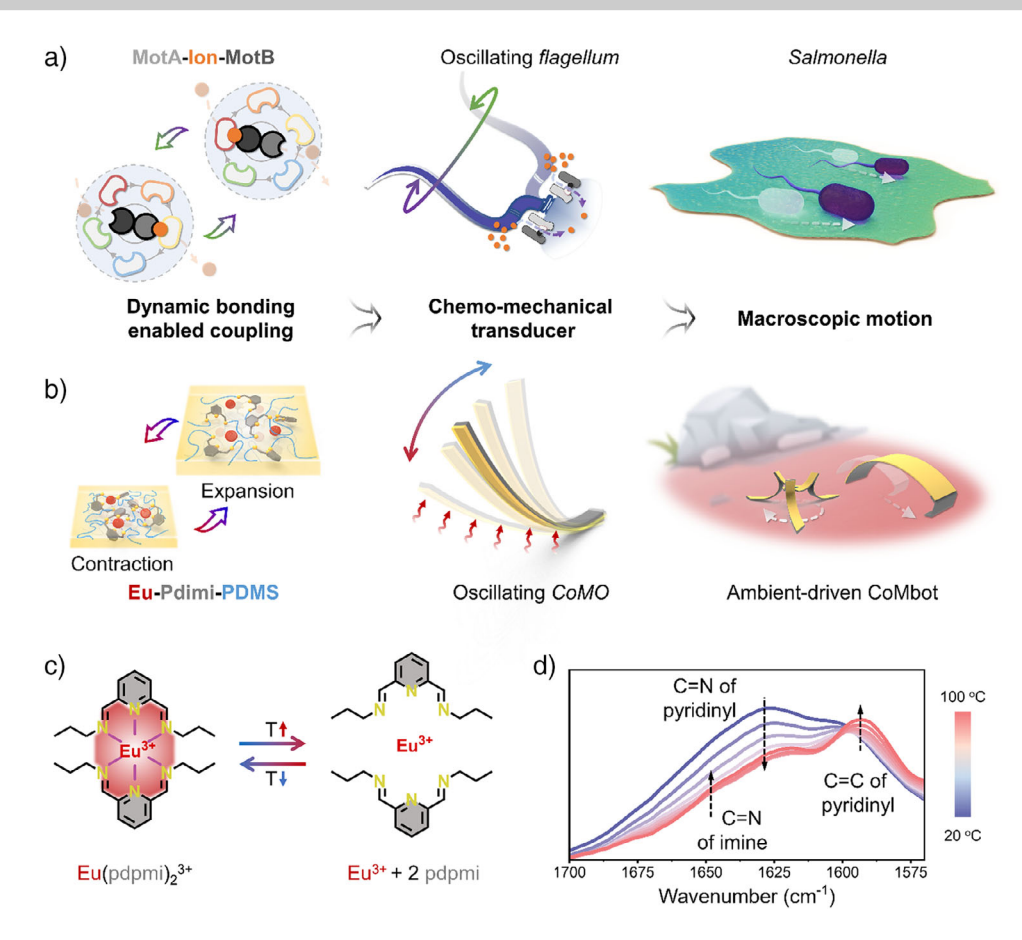


Figure 1. Schematic illustration depicting the oscillating CoMO and autonomous CoMbot inspired by the self-sustained moving flagella of Salmonella. a) Microscopic mechanism showing the oscillation of flagella is maintained by the torque generated by chemo-mechanical coupling of proteins on the cell membrane, which originates from the reversible dynamic coordination of ion (H⁺ or Na⁺) binding between MotA protein and MotB protein. b) Biomimetic oscillation of CoMO, which is mainly derived from the chemo-mechanical coupling, enabled repeating thermal inflation and contraction of active layer material (Eu-Pdimi-PDMS) that was guaranteed by highly reversible dynamic Eu-Pdimi coordination interaction. c) The structure shows the reversible disassociation and association of Eu(pdpmi)₂³⁺ while temperature fluctuates. d) Temperature-correlated FT-IR spectrum of Eu(pdpmi)₂³⁺.

In sharp contrast, natural microorganisms have evolved fundamentally different self-sustained motion mechanisms capable of harvesting low-density ambient energy at the molecular level and transducing molecule transitions into macroscopic movement. For example, Salmonella is known to actively harness the energy from its constant surroundings to produce self-sustained periodic movement of its flagella, thus efficiently locomoting in various environments (Figure 1a). Recent studies have revealed that their flagella are chemo-mechanical transducers that are propelled by protein nanomotors composed of a central stator surrounded by several rotor units.[41-43] The oscillation of the flagellum is primarily generated by the torque produced by MotA₅B₂ complexes. This assembly comprises a unique asymmetric 5:2 subunit stoichiometry, creating a chemo-mechanical coupling between the two MotB units in the dimer, whereby only one MotB unit can bond with MotA at one time. When there is a constant ion flow (mainly Na⁺ or H⁺), the MotA ring would rotate through alternatively formed MotB-ion-MotA interactions between the MotB dimer and the surrounding five MotA subunits. More importantly, it is the dynamic MotBion-MotA bond that ensures the alternated association and dissociation happen and thus maintains the oscillation. Such highly dynamic bonding-enabled chemo-mechanical coupling offers a more promising approach to the development of artificial motors with enhanced energy harvesting ability and adaptability in low-energy-density natural environments.

To replicate such bio-like ambient-driven motion, the key lies in engineering highly dynamic soft materials to complete chemo-mechanical coupling for harvesting surrounding trivial energy and inducing macroscopically self-sustained motion. Herein, as a prototype, we achieve self-excited oscillation by harnessing the dynamic coordination between Europium ions (Eu³⁺) and 2,6-pyridinediimine (Pdimi), which speedily dissociates upon minor heating and associates upon cooling in a highly reversible manner (Figure 1b). Embedding such a dynamic transition into polydimethylsiloxane (PDMS) polymer network results in a supramolecular elastomer that is dynamically crosslinked by Eu³⁺ (Eu-Pdimi-PDMS). Integrating dynamic Eu-Pdimi-PDMS material as the active layer with commercially available cellulose papers as the passive layer forms a Coordination-motorized oscillator (CoMO). The highly dynamic Eu-Pdimi crosslinks within the active layer endow it with an exceptionally large thermal



sensitivity, whose expansion coefficient is 25-fold that of normal PDMS and nearly 2000-fold that of the passive layer. The biomimetic self-sustained oscillation of CoMO is achieved by harnessing ambient heat for reversibly binding and breaking the Eu-Pdimi coordination crosslinks in the active layer and transducing such molecular transition into macroscopic oscillation through chemo-mechanical coupling, akin to the molecular motor of bacterial flagella. Ambient heat, as low as body heat, can be harnessed and transformed into continuous mechanical output. Further investigations revealed that such a principle can be extended to versatile systems by replacing Eu³⁺ with other metal ions (e.g., Al³⁺, Zr⁴⁺) to form reversible coordination interactions. Finite element analysis (FEA) simulation models were developed to illustrate the contribution of individual material properties to oscillation, providing valuable guidance for subsequent chemistry design. The universal design principles underlying dynamic lanthanide coordination chemistry have facilitated structural enrichment to amplify motion, diversify motion patterns, and upgrade motion-to-locomotion transitions. These advancements are realized in chemo-mechanical coupled oscillatory systems that function as motors, exemplified by the development of untethered soft robots known as CoMbots (Coordination Motorized Robots) with multi-terrain adaptability, tunable speed, and customizable postures. The feasibility of the chemo-mechanical transition mechanism allows the efficient utilization of low-density ambient heat sources, such as solar energy stored on surfaces and waste heat from electronics, for locomotion. These findings underscore the transformative potential of dynamic chemical transitions in creating chemo-mechanical coupling systems. By translating molecular-scale processes into macroscopic energy outputs, these systems pave the way for robust, biomimetic, and sustainable soft machinery with unparalleled capabilities in energy conversion and adaptability.

Results and Discussion

From Molecular Transition to Macroscopic Oscillation

As a prototype, the coordination interaction was selected for designing highly dynamic materials because its dynamicity can be easily tuned by varying the central ion and ligand across a wide range. The Europium ion (Eu³⁺) coordinated 2,6-pyridinediimine-functionalized PDMS (Eu-Pdimi-PDMS) was designed and synthesized as a prototype active material for self-sustained oscillations. To understand the dynamic nature of the Eu-Pdimi coordination interactions, a model compound, 1,1'-(pyridine-2,6-diyl)bis(N-propylmethanimine) (pdpmi), was synthesized and its Eu³⁺ coordinated behavior was systematically investigated (Figures 1c and S1). According to the hard-soft-acid-base theory, Eu³⁺ is a hard Lewis acid while the N-containing pdpmi ligand is a moderate Lewis base, suggesting that the Eu³⁺-pdpimi coordination bonds are relatively weak. Meanwhile, pdpmi, as a multidentate ligand, could form multiple coordination bonds with Eu³⁺ simultaneously and emit an energy of 866.9 kJ mol⁻¹ according to density functional theory (DFT) simulation,

indicating a high tendency for association. Thus, the highly reversible MotA-ion-MotB in flagella could be well replicated by Eu-pdpmi complex. To further confirm their dynamicity, the temperature-dependent Fourier transform infrared (FT-IR) studies of the Eu³⁺-pdpmi complex were conducted. As depicted in Figure S2, upon coordination with Eu³⁺, significant blue shifts were observed in both the C=N stretching vibration (from 1585 to 1622 cm⁻¹) and pyridinyl C=C stretching vibration (from 1567 to 1597 cm⁻¹) at room temperature. With increasing temperature, these blue-shifted peaks demonstrated backward shifts, suggesting the gradual breakage of Eu³⁺-pdpmi coordination bonds at high temperatures (Figure 1d). As the temperature dropped back to 20 °C again, these peaks would be recovered (Figure S3). Perturbationcorrelation moving window (PCMW) (Figure S4), which was calculated from temperature-correlated FT-IR spectra, revealed that the dissociation of Eu³⁺-pdpmi started at ~22 °C, changed fastest at 30 °C, and then slowed down after reaching 40 °C.[44] Bond energy calculated from DFT simulation result also confirmed the weak and dynamic coordination bonds between Eu³⁺ and pdpmi (Figure S5 and Table S1).

By introducing such Eu-pdpmi dynamic coordination bonds into the PDMS elastomer network as dynamic physical crosslinks, it endows the elastomer with a dynamic nature of Eu-Pdimi-PDMS polymer network (Figures 2a,b and S6). The synthesized Pdimi-PDMS with $M_w \sim 17~700~{\rm g~mol^{-1}}$ was a viscous liquid at room temperature but solidified after the introduction of Eu³⁺. X-ray photoelectron spectroscopy (XPS) results confirmed the successful coordination between Eu³⁺ and Pdimi ligand (Figures S7 and S8). As demonstrated in Figure 2c, the storage modulus (G') of Eu-Pdimi-PDMS was enhanced by 25000-fold as the frequency rose from 10^{-4} Hz to 10^2 Hz. Its relaxation time (τ) was further obtained through their master curves from 20 to 80 °C (Figure S9). The results (Figure 2d) showed that the relaxation time (τ) at 20 °C was about 10 s, suggesting the fast coordination bond exchanges within the polymer network at room temperature in comparison with the stable metal coordination bonds (>100 s).[45,46] When the temperature was raised to 60 °C, the coordination bond exchange accelerated significantly and the relaxation time was largely shortened to 0.45 s, indicating a highly dynamic nature contributed to profound temperature sensitivity. Temperature-dependent rheology test showed that the G' of Eu-Pdimi-PDMS $([Eu^{3+}]/[Pdimi] = 25/1)$ was 1.9×10^4 Pa at 20 °C but declined steeply in the temperature range of 50 –110 °C and reduced to 36 Pa at 120 °C (Figure 2e). The mechanical property switch ratio (δ, defined as $G'_{20\,^{\circ}C}/G'_{120\,^{\circ}C}$) was calculated to be more than 500 within the 100 °C temperature variation. [47] These results suggested that the significant temperaturedependent mechanical property variation should originate from the highly temperature-sensitive Eu-Pdimi coordination crosslinks. As illustrated in Figure 2b, when the material was heated up, the equilibrium of $Eu^{3+} + Pdimi \leftrightarrow Eu^{3+} - Pdimi$ shifted toward the dissociation state, generating more uncrosslinked Pdimi-PDMS chains to reduce the mechanical modulus. Based on the intersection frequency of G' and G" scanned at various temperatures, Arrhenius plots were estimated to show that the apparent activation energy (E_a)

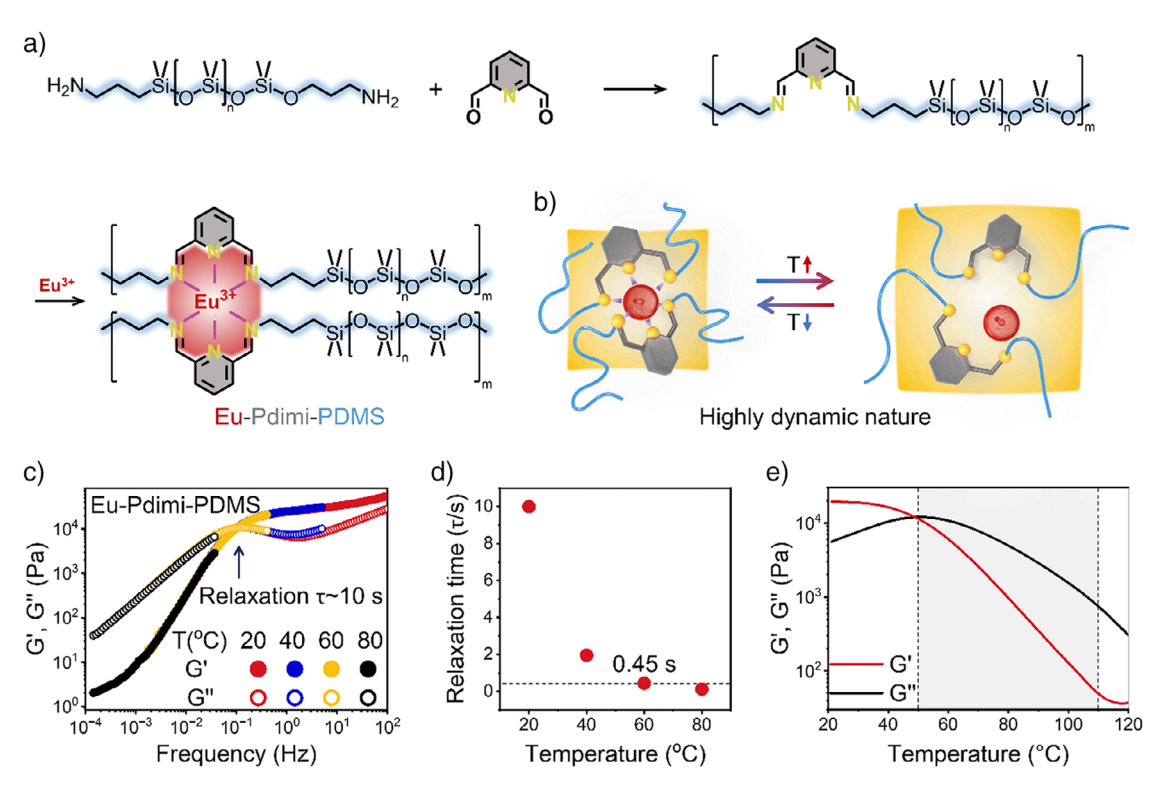


Figure 2. Highly dynamic nature of Eu-Pdimi-PDMS. a) Synthesis and structure of Eu-Pdimi-PDMS. b) Schematic illustration of Eu-Pdimi-PDMS undergoing reversible dissociation and reform as temperature rises and drops. c) Master curve of Eu-Pdimi-PDMS at a reference temperature of 20 °C, prepared by the time-temperature superposition treatment of storage modulus (G') and loss modulus (G'') values obtained at 20, 40, 60, and 80 °C. d) Relaxation times of Eu-Pdimi-PDMS, estimated from the crossover points of G' and G" at various temperatures. e) Variation in G' and G" of Eu-Pdimi-PDMS as a function of temperature.

for the slippage of Eu-Pdimi-PDMS was as low as 58 kJ mol⁻¹ (Figure \$10). For the Eu-Pdimi-PDMS network, polymer chains presumably slipped and interpenetrated by breaking their Eu-Pdimi coordination bonds. As a result, the interchain interactions easily weakened with increasing temperature, which contributed to a large thermal expansion of Eu-Pdimi-PDMS. As shown in Figure S11, the average linear thermal expansion coefficient (α) of Eu-Pdimi-PDMS within 20 -100 °C is 6.38×10^{-3} K⁻¹, which is over 25-fold that of the commercially chemical-crosslinked PDMS (chem-PDMS, $0.25 \times 10^{-3} \,\mathrm{K}^{-1}$).[48]

By integrating with highly thermal-stable but flexible material, cellulose paper, a coordination-motorized oscillator (CoMO) that could constantly harvest ambient heat for translating molecular transition into macroscopic oscillation was developed (Figure 3a.b). The CoMO could demonstrate stable oscillation autonomously on an isothermal heat source (~60 °C) with an oscillation frequency of 0.18 Hz and amplitude of 17°, which shows good accordance with FEA results (Figure 3c). Real-time bending angle and surface temperature on central of CoMO were recorded in Figure 3d, where the oscillation of CoMO shows an obvious correlation and a constant delay to the perturbation of its surface temperature.

Due to the highly dynamic polymer network of Eu-Pdimi-PDMS, such a transition mechanism can be attributed to the highly dynamic supramolecular interaction, enabling chemomechanical coupling as elucidated in Figure 3a,b. At the initial state, both the Eu-Pdpmi-PDMS and cellulose paper layers were heated to expand due to the constant heat source. Owing to the 1700-fold expansion coefficient difference between Eu-Pdimi-PDMS and cellulose paper layers (Figure \$11), large kinetic energy was generated, causing the CoMO to quickly deform against the Eu-Pdimi-PDMS layer. Thus, the tip of CoMO quickly bends upward and overshoots the mechanical equilibrium position (state I), where the Eu-Pdimi coordination was fully broken, leading to excessive bending. The overbending drives the whole actuator further distant the heat source. Thus, the actuator temperature starts to drop during state I-state II. Although the temperature drop caused recovery of the Eu-Pdimi crosslinking and gradual contraction of the active layer, the actuator still over-bended to state II and thus transfers the remaining kinetic energy into elastic energy. Such out-of-equilibrium over-bending, along with the subsequent under-bending, is driven by the actuation inertia and enabled by the stimulusresponse time lag, which is the delay between stimulus input and material response. In our system, this lag arises from the intrinsic polymer viscoelasticity of active layer material and the temporal mismatch between heat absorption and actuation force generation, as the heat is primarily absorbed at the outer air-solid surface, while the actuation force arises from the inner active-passive layer interface. It takes time for the heat to penetrate through the thickness elibrary.wiley.com/doi/10.1002/anie.2023/18011 by University of California, Los Angeles, Wiley Online Library on [06/11/2025]. See the Terms and Conditions (https://onlinelibrary.wiley.com/terms-and-conditions) on Wiley Online Library for rules of use; OA articles are governed by the applicable Creative Commons License

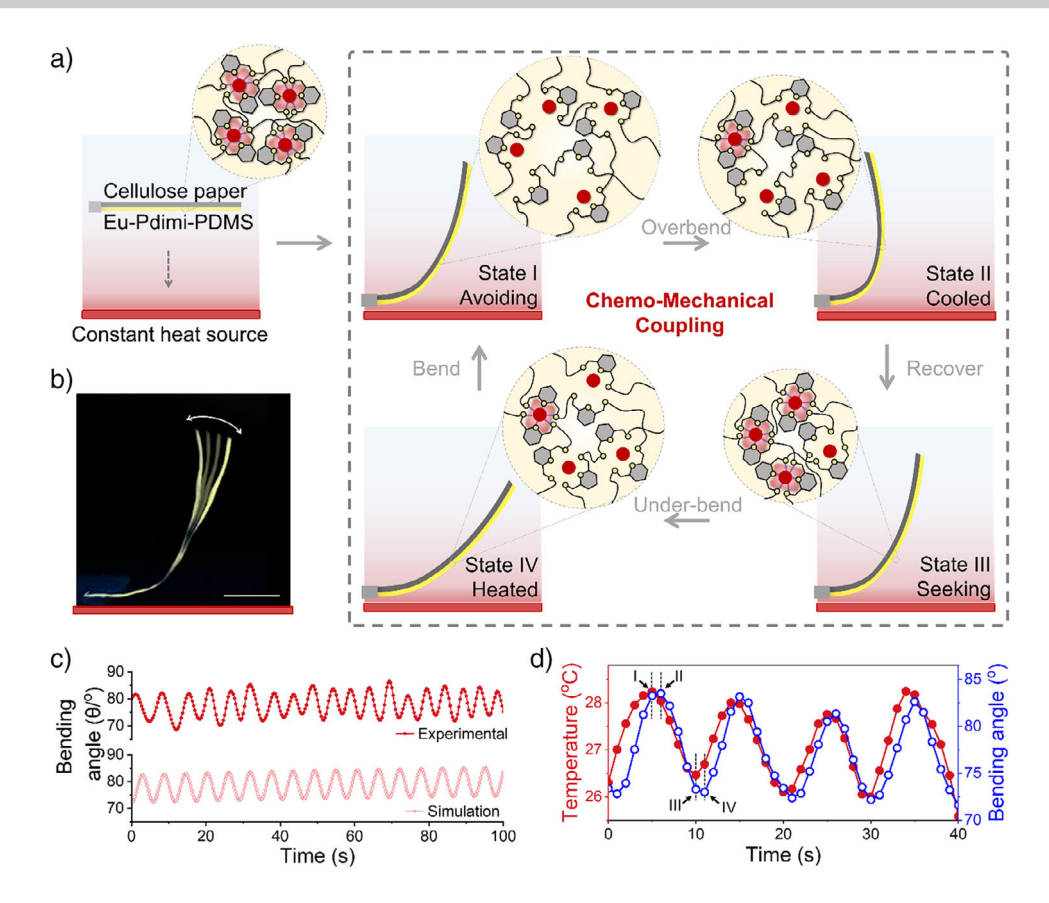


Figure 3. Dynamic bonding enabled chemo-mechanical coupling that transfers molecular transition into macroscopic oscillation. a) Schematic illustration of the built-in chemo-mechanical coupling mechanism of CoMO. b) Image and c) time-resolved bending angle of oscillating CoMO on a 60 °C isothermal heat source. Scale bar: 5 mm. d) Real-time tracking of surface temperature and bending of CoMO on a 60 °C isothermal heat source, which shows obvious chemo-mechanical coupling.

of the structure. The characteristic thermal timescale τ is inversely proportional to the material's thermal conductivity k. Given the intrinsically low k of polymeric materials, this results in a relatively long delay (large τ) before significant through-thickness temperature gradients are established. Consequently, the generation of internal thermal strain, stress, and bending moment that drives deformation and oscillation is also delayed. Together, the viscoelastic relaxation and the thermal-diffusion delay produce the temporal mismatch between heat absorption and force generation. This delayed response allows the actuator to overshoot the mechanical equilibrium position under the influence of inertia, thereby producing the observed overbending. At state II, the tip was at the highest position with the largest elastic energy. Then, the release of elastic energy drives the actuator tip to bend back toward the heat source. The decline of actuator temperature resulted in the active layer contraction and provided the actuator with enough kinetic energy to overcome the mechanical equilibrium position again at stage III, at which the Eu-Pdimi bonding was mostly recovered. After that, driven by inertia, the actuator further got closer to the heat source until reaching the lowest position (state IV), and the actuator temperature starts to rise between state III and state IV. State IV was the lowest position, where the elastic energy reached maximum again and kinetic energy was fully exhausted. With the CoMO close to the hot surface, its temperature drastically increased, which caused the dissociation of Eu-Pdimi coordination bonds and inflated the active layer again. Thus, the CoMO bent up again toward state I to start the following cycles of sustained oscillation. In such a process, the bonding status of Eu-Pdimi was highly coupled with the mechanical bending status of CoMO: debonding, bending \rightarrow bonding, overbending \rightarrow bonding, recover \rightarrow debonding, under-bending \rightarrow next cycle, forming a self-sustained chemo-mechanical coupling that efficiently transfers molecular transition to macroscopic oscillation.

It is worth noting that the temperature variation between the highest and lowest oscillation positions is only around 2 °C (Figure 3d). Such a minimal temperature difference would typically be ineffective for conventional material-based thermal expansion actuators. In contrast, CoMO can harness such a small energy differential to continuously generate mechanical output, with energy-to-work output conversion efficiency comparable to that of the light-driven liquid crystal elastomer oscillators (Figure S12), thanks to the highly dynamic bonding of the Eu-Pdimi-functionalized PDMS active layer and embedded chemo-mechanical coupling, which are exceptionally effective to even slight changes in temperature.

elibrary.wiley.com/doi/10.1002/anie.202518011 by University Of California, Los Angeles, Wiley Online Library on [0611/2025]. See the Terms and Conditions (https://onlinelibrary.wiley.com/terms-and-conditions) on Wiley Online Library for rules of use; OA articles are governed by the applicable Creative Commons License

elibrary.wiely.com/doi/10.1002/anie.202518011 by University Of California, Los Angeles, Wiley Online Library on [06/11/2025]. See the Terms and Conditions (https://onlinelibrary.wiely.com/terms

-and-conditions) on Wiley Online Library for rules of use; OA articles are governed by the applicable Creative Commons License

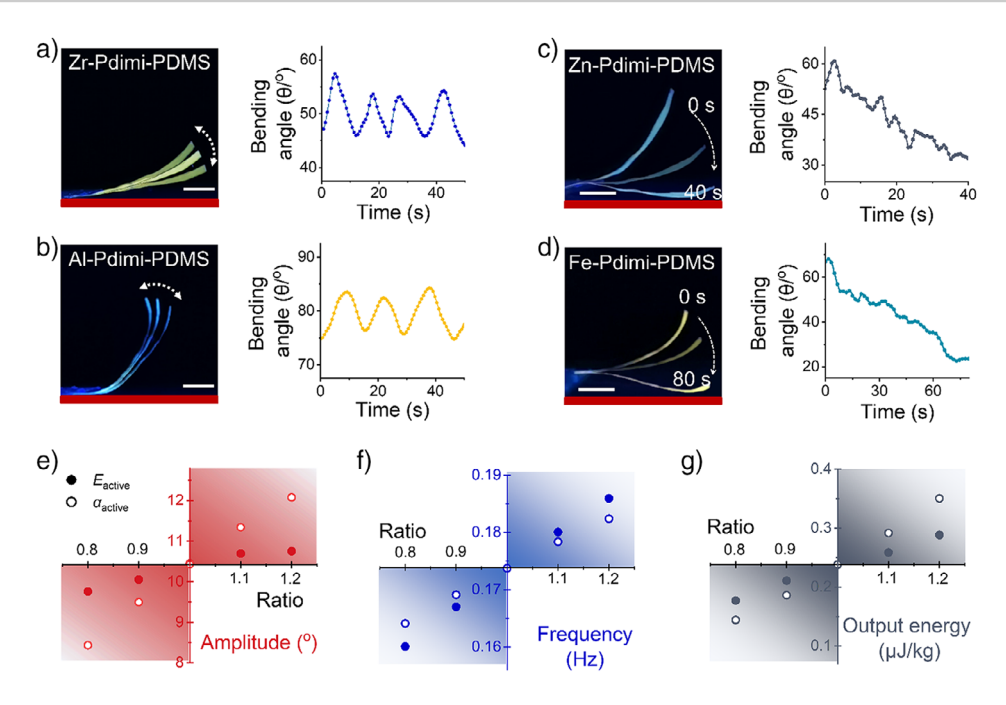


Figure 4. Influence of bonding dynamics on chemo-mechanical coupling. Image and time-resolved bending angle of oscillating a) Zr-Pdimi-PDMS actuator, b) Al-Pdimi-PDMS, c) Zn-Pdimi-PDMS actuator, d) Fe-Pdimi-PDMS actuator on 60 °C isothermal heat source. The effects of the modulus and thermal expansion coefficient (α) of active-layer materials on oscillation e) amplitude, f) frequency, and g) output energy are revealed by finite element simulations. Both parameters were varied by the same percentage (±10% and ± 20%) around the same baseline.

Guided by the dynamic interaction enabled by chemomechanical coupling, in addition to the CoMO of Eu-Pdimi-PDMS, oscillating systems are promised to be extended by using other metal ions (Fe³⁺, Zn²⁺, Al³⁺, and Zr⁴⁺) to crosslink Pdimi-PDMS (Movie S1). Analogous to the Eu-Pdimi-PDMS, self-sustained oscillation was also observed in Al-Pdimi-PDMS and Zr-Pdimi-PDMS systems because the rapid dissociation of Al-Pdimi and Zr-Pdimi coordination crosslinks occurred above 22 and 40 °C, respectively (Figures 4a,b and S13). Nevertheless, they performed slowerfrequency (0.082 and 0.073 Hz for Al-Pdimi-PDMS and Zr-Pdimi-PDMS actuators, respectively) and lower-amplitude (7.2° and 8.4° for Al-Pdimi-PDMS and Zr-Pdimi-PDMS actuators, respectively) oscillations compared to Eu-Pdimi-PDMS actuator (a frequency of ~0.18 Hz, an amplitude of $\sim 12.0^{\circ}$). This performance difference was rooted in the differential temperature sensitivity of these active-layer materials. Specifically, temperature-triggered mechanical property switching and thermal inflation ability of Al-Pdimi-PDMS (δ = 61, α = 1.21 \times 10⁻³ K⁻¹) and Zr-Pdimi-PDMS (δ = 67, α $= 9.30 \times 10^{-4} \text{ K}^{-1}$) are much weaker than those of Eu-Pdimi-PDMS ($\delta = 527$, $\alpha = 6.38 \times 10^{-3} \text{ K}^{-1}$) (Figure S14). In sharp contrast, no self-sustained oscillation was observed for Zn-Pdimi-PDMS and Fe-Pdimi-PDMS actuators (Figure 4c,d) due to negligible temperature-triggered mechanical property switching and much smaller thermal inflation ratio for much higher triggering temperatures (Figures S15 and S16). Such a distinct phenomenon is rooted in their molecular dynamicity. DFT calculations revealed that the bond energies of Fepdpmi and Zn-pdpmi coordination bonds are much larger than those of Al-pdpmi and Zr-pdpmi, while the Eu-pdpmi coordination bond is the weakest (Figure \$17 and Table S1). These results proved our hypothesis that highly dynamic metal coordination crosslinks were the key to generating sufficient thermal inflation capability as the active layer, thus enabling the chemo-mechanical coupling for realizing macroscopic self-sustained oscillation.

Similarly, crosslinking density also determines the material dynamicity. We varied the crosslinking density by adjusting the Eu³⁺/Pdimi ratio to fabricate a series of bilayer actuators. Their self-sustained oscillation behaviors were evaluated by parallelly placing them along a constant-temperature hot surface (60 °C). As can be seen from Figure \$18, no heat-activated deformation was observed for the actuator prepared from the non-crosslinked Pdimi-PDMS, demonstrating the indispensable importance of Eu-Pdimi crosslinks. With increasing Eu-Pdimi crosslinks by raising the Eu³⁺/Pdimi molar ratio from 1/100 to 1/50, the free actuating end could bend up but soon descend back to the initial position without continuous oscillation. At the appropriate ratio of Eu-Pdimi crosslinks (Eu³⁺/Pdimi molar ratio was 1/25–1/12), stable and continuous oscillation behaviors were clearly observed. However, if there were too many Eu-Pdimi crosslinks (Eu³⁺/Pdimi molar ratio was 1/5–1/2), such self-sustained oscillation could not last either. The Eu-Pdimi-PDMS with Eu/Pdimi = 1/25and 1/12 have higher mechanical property switch ratios δ as the temperature rises, thus resulting in more significant thermal expansion coefficients than other Eu-Pdimi-PDMS samples. Consequently, larger driving forces were generated to trigger the chemo-mechanical coupling for sustaining the oscillation.

As evidenced by our results, the chemo-mechanical coupling is strongly influenced by the dynamicity of the involved molecule transition, which is reflected by thermal

15213773, 0, Downloaded from https://onlinelibrary.wiley.com/doi/10.1002/anie.202518011 by University Of California, Los Angeles, Wiley Online Library on [06/11/2025]. See the Terms and Conditions (https://onlinelibrary.wiley.com/terms-and-conditions) on Wiley Online Library for rules of use; OA articles are governed by the applicable Creative Commons License

Research Article

expansion ability at the macroscopic level. It is also well known that increasing material rigidity could potentially enhance the oscillation due to its contribution to stress mismatch between the active and passive layers, facilitating bending. Therefore, it is crucial to distinguish the contribution and weight of material properties to oscillation behavior (amplitude, frequency, and output energy). To address this, we conducted finite element simulations to reveal the effects of the modulus (E) and thermal expansion coefficient (α) of active-layer materials on oscillation performance. The Eu-Pdimi-PDMS/cellulose paper system, which exhibited optimal performance, was selected as the reference (baseline). We varied the modulus (E_{active}) and thermal expansion coefficient (α_{active}) of the active-layer material by the same percentage $(\pm 10\%$ and $\pm 20\%$) to explore their relative importance (impact weight). By adjusting E_{active} and α_{active} from -20% to + 20%, we observed enhanced oscillation amplitude (defined as θ_{max} - θ_{min}), frequency, and output energy as shown in Figure 4e-g. A higher α_{active} generates larger thermal stresses $\sigma_{\rm th}$ and strains $\varepsilon_{\rm th}$ ($\sigma_{\rm th} = E_{\rm active} \varepsilon_{\rm th} = E_{\rm active} \alpha_{\rm active} \Delta T$), effectively expanding the active material. This increase also leads to a larger stress mismatch between the active and passive layers, which facilitates the bending of our oscillator. An increase in E_{active} also has the same effect, but it additionally enhances the flexural rigidity of the structure (D = EI, where I is the moment of inertia), which is not beneficial for bending amplitude but can result in a higher oscillation frequency. Therefore, while both properties are influential, the influence of E_{active} on oscillation amplitude and output kinetic energy density (defined as $E_k = (1/m) \int 0.5 \rho v^2 dV$) is less pronounced compared to α_{active} . However, it is challenging to decouple these properties in experiments as the α and E represent the material dynamicity and robustness, respectively, which are typically contradictory properties. In this scenario, our simulation further emphasizes that improving material dynamicity should be a higher priority due to its higher relative importance.

We also revealed the influence of passive layer properties on the oscillation behavior of CoMO (Figure S19). Our simulation results indicate that increasing the stiffness of the passive layer (E_{passive}) not only reduces the stress mismatch but also increases the flexural rigidity, both of which hinder oscillation. In contrast, adjusting the thermal expansion coefficient $(\alpha_{\text{passive}})$ within a range of -20% to + 20% does not significantly impact the oscillation behavior, including amplitude, equilibrium position, and kinetic energy density. This suggests that further improvements in oscillation performance can be achieved by using more flexible materials without concern for their higher α_{passive} values compared to cellulose paper.

Environment Adaptability and Universality

Since the dynamic polymer network of the active Eu-Pdimi-PDMS material is sensitive to temperature, oscillation performances of the actuators are expected to be facilely controlled by regulating the surface temperature (T_{surf}) (Figure 5a). As demonstrated in Figure 5b, the oscillation can be observed at $T_{\text{surf}} = 30$ °C. As T_{surf} increases, both

the oscillating amplitude and frequency of CoMOs (width = 1 mm, length = 25 mm) are boosted. This is because the higher temperature will result in much faster dissociation of the Eu-Pdimi coordination crosslinks to provide the free actuating end with larger kinetic energy. The optimized operation temperature is about 60–70 °C. When T_{surf} is over 70 °C, the oscillation amplitude will be compromised because the overheated heat source may restrict the bending back process. Results demonstrated that stable oscillation of the CoMOs can be triggered by using the constant-temperature heat surface of 30-100 °C. Wide operation temperature endows CoMO with good environmental adaptability and the capability of harvesting various heat resources for activating molecular transition and generating macroscopic oscillation. For example, the CoMO can even utilize heat emitted by the hand for self-sustained oscillation (Figure 5c and Movie S2). Other operation conditions and CoMO features have also been optimized (Figure \$20).

Having optimized the ideal material composition, geometrical dimensions, and oscillation conditions for CoMOs, the oscillation stability was investigated in detail. Initially, the CoMO (active layer thickness ~32 μm, 25 mm length, 1 mm width) was positioned near the heating surface (T_{surf} = $60 \, ^{\circ}$ C, gap = 1 mm). As summarized in Figure S21, the stable oscillation was monitored for over 6 h. It was found that the oscillation could sustain 550 cycles during the first hour without performance loss. After 2 hours, only a slight decline of the oscillating amplitude was observed. Remarkably, the oscillator could further keep stable and continuous oscillation for more than 4000 cycles in the following 5 hours. The chemical composition of Eu-Pdimi-PDMS was also confirmed to remain stable (Figure \$22).

In addition to the typical flapping-like oscillation, which generates directional work output through single up-anddown movements, other motion patterns can be readily achieved by rational geometry programming for multi-modal work output. For instance, by shaping the CoMO into a helical form, it can produce reciprocal motion in the vertical direction through an oscillating twist-and-de-twist process (Figure 5d and Movie S3). Beyond directional movement, other forms of work output can be realized through strategic system integration. As shown in Figure 5e and Movie \$3, the free end of the CoMO is connected to a gear, allowing the continuous flapping oscillation mode to be translated into repetitive spinning, delivering a sinusoidal torque output. Such multi-modal oscillation ability proves the robustness and universality of chemo-mechanical coupling.

Amplification of Oscillation

More effective chemo-mechanical transition can be achieved through rational structure design to amplify macroscopic motion. The joint-muscle architecture, as the collective work of each muscle between the joints, has already been proven to be critical for natural beings to magnify the morphing amplitude.[49] As illustrated in Figure 5f and Movie S4, one collective oscillator was constructed through a series connection of three identical CoMOs with a length of 7 mm.

://onlinelibrary.wiley.com/doi/10.1002/anie.202518011 by University Of California, Los Angeles, Wiley Online Library on [06/11/2025]. See the Terms and Conditions (https://onlinelibrary.wiley.com/terms

and-conditions) on Wiley Online Library for rules of use; OA articles are governed by the applicable Creative Commons License

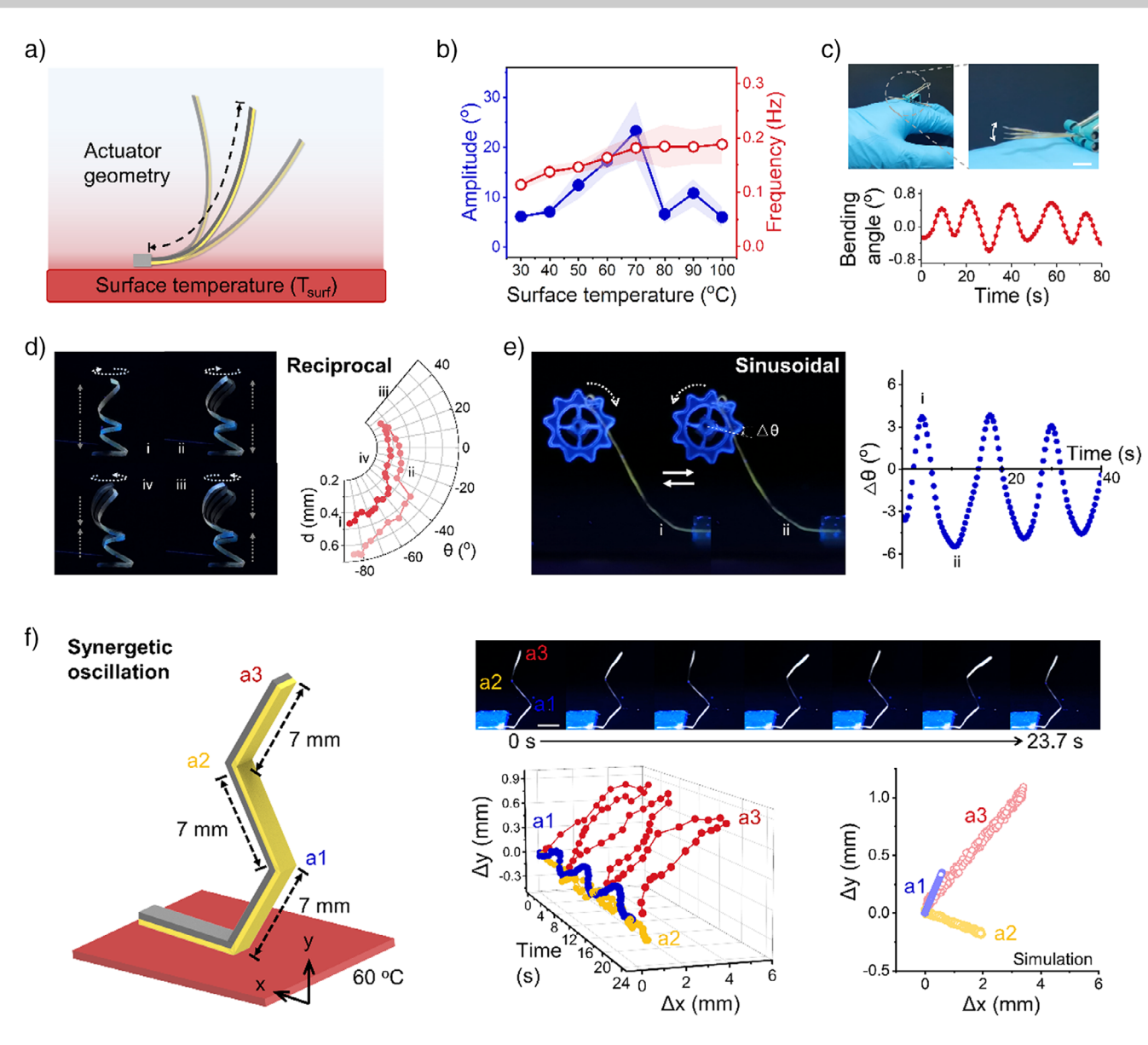


Figure 5. Adaptability, universality and amplification of chemo-mechanical coupling enabled oscillation. a) The schematic illustration shows the main factors that regulate the oscillation of CoMO. b) Oscillation amplitude and frequency of CoMO on an isothermal surface with different temperatures, showing the wide temperature adaptiveness of chemo-mechanical coupling. Error bars indicate the standard deviation of the mean values obtained from 5 independent samples. c) Harnessing body heat for self-sustained oscillation. Universality of chemo-mechanical coupling demonstrated by d) reciprocal oscillating motion of helical-shaped CoMO and e) sinusoidal torque output of CoMO-gear system. f) Image of amplified chemo-mechanical coupling oscillation achieved by the synergetic effect of end-by-end connected CoMOs and its corresponding time-resolved displacement status. Scale bar: 5 mm.

Consequently, the oscillating amplitude of its free end (a3, $\Delta x_{\rm max} = 5.27$ mm, $\Delta y_{\rm max} = 0.89$ mm) was largely amplified by 4-fold due to the collective effect of three series-connected oscillators, in comparison with that of the bottom actuator (a1, $\Delta x_{\rm max} = 0.24$ mm, $\Delta y_{\rm max} = 0.13$ mm). Remarkably, it was proven that oscillating amplitude could be further amplified by the series connection of more CoMOs (Figure S23). Besides, it was also possible to expand the degree of freedom (DOF) oscillation pattern through the series connection of CoMOs. As shown in Figure S24, the collective effect of seven series-connected CoMOs was capable of transforming the homodromous oscillation into an upwards-magnifying oscilla-

tion in divergent directions. Such largely enlarged oscillation amplitude and DOF could generate more considerable force, which laid the foundation for utilizing the chemo-mechanical coupling propelled CoMO as motors to accomplish practical tasks such as object shifting (Figure \$25 and Movie \$5) or autonomous locomotion.

Autonomous Coordination-Motored Robots (CoMbots)

Chemo-mechanical coupling enabled self-sustained oscillations could also be utilized for robotic movement that is

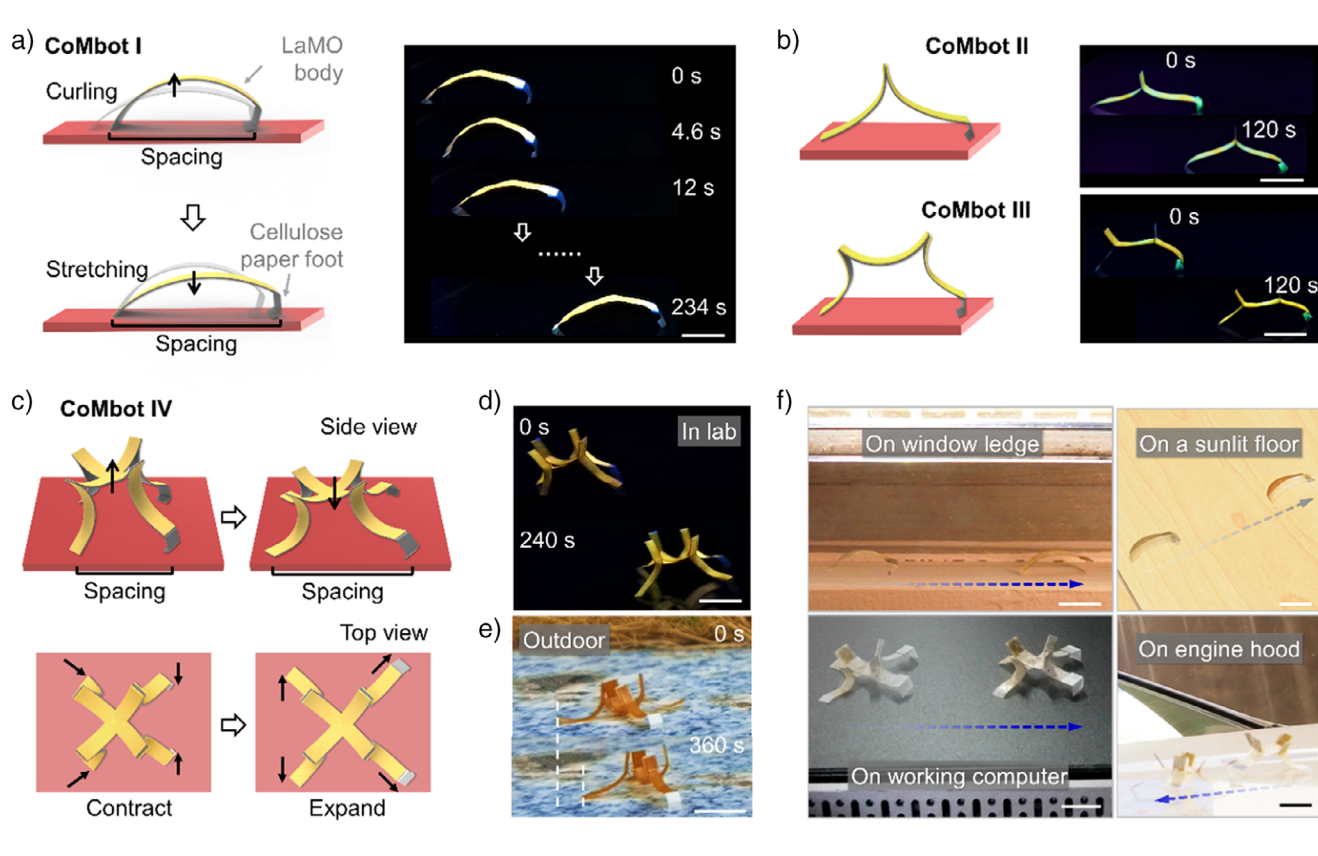


Figure 6. Chemo-mechanical coupling enabled ambient-driven autonomous walking CoMbots. a) Mechanism and images of autonomous unidirectional inchworm-like walking achieved by CoMbot I. b) Scheme and images demonstrate the autonomous unidirectional locomotion of CoMbot II and CoMbot III with higher locomotion speed. c) Schematic illustration and images of autonomous unidirectional octopus-like movement of the cross-shaped soft robot, CoMbot IV. Locomoting CoMbot IV on d) a simulated isothermal heat source and e) using outdoor ambient heat for autonomous locomotion. f) CoMbot autonomously moves on a window ledge, sunlit floor, operating computer, and car engine hood by harnessing ambient or wasted heat. Scale bar: 10 mm.

fuelled by ambient heat. We developed various walking CoMbots in four generations, from CoMbot I to IV. Walking CoMbot I featured a single CoMO attached to a paper foot. When placed on the isothermal glass surface (60 °C), it could achieve self-continuous inchworm-like motion due to asymmetric friction. The periodic curling-stretching process of the back foot propelled the walking CoMbot forward. After 20 oscillating cycles within 240 s, its back foot could move forward over 23 mm (Figure 6a, Movie S6). We further examined the influence of body length on locomotion performance. The results show that increasing body length leads to slower oscillation frequency but larger displacement per cycle (Figure S26).

Since end-by-end connected CoMOs could enhance the oscillation properties, we hypothesized that the autonomous walking performance would be improved by similar end-by-end connected designs. Walking CoMbots II and III, with the same body length as walking CoMbots I, were fabricated with two and three end-by-end connected CoMbots, as presented in Figure 6b. Compared to the CoMbots I, walking CoMbot II demonstrated higher oscillation frequency and larger spacing variation due to the collective effect, leading to a 15% increase in speed. Similarly, walking CoMbot III further enhanced its speed by 16% compared to walking CoMbot II (Figure S27).

To expand the locomotion mode, walking CoMbot IV was assembled using four stripe-shaped CoMbots as legs and one cross-shaped CoMbot (Figure 6c). To achieve better control of unidirectional locomotion, two paper-made feet were adhered to the ends of two adjacent legs. When placed on the isothermal surface, four stripe-shaped legs periodically bent and unbent to generate up-down oscillation, resulting in autonomous and unidirectional octopus-like locomotion. As shown in Figure 6d and Movie S7, walking CoMbot IV could locomote over 22 mm within 240 s, exhibiting an average oscillation frequency of ~ 0.08 Hz and an average spacing change of ~ 4.2 mm per cycle. Notably, such soft walkers can perform stable locomotion not only on low-friction glass surfaces but also on rough paper cards or gravel lands with obstacles, suggesting multi-terrain adaptation (Figure \$28 and Movie \$8). More astonishingly, walking CoMbot IV was capable of harnessing ambient thermal energy for sustaining chemo-mechanical coupling. As shown in Figure 6e and Movie \$9, it could autonomously locomote on the outdoor granite bricks beside the sidewalk on a summer day (recorded in Ningbo, Aug. 21, 2022, 34 °C). Additionally, we conducted tests on CoMbots across diverse real-world settings to assess their adaptability in harnessing various ambient heat sources. As shown in Figure 6f and Movie S9 (recorded in Los Angeles, Oct. 29, 2024, at 25 °C), CoMbots successfully 2/onlinelibrary.wiley.com/doi/10.1002/anie.202518011 by University Of California, Los Angeles, Wiley Online Library on [06/11/2025]. See the Terms and Conditions (https://onlinelibrary.wiley.com/terms-and-conditions) on Wiley Online Library for rules of use; OA articles are governed by the applicable Creative Commons Licensea

utilized solar energy and residual wall heat after sundown to achieve autonomous locomotion. Waste heat from electronics and machinery (e.g., a computer and a car engine hood) was also effectively captured to sustain their movement. These findings highlight the adaptability of dynamic Eu-Pdimi interaction, which ensuring the chemo-mechanical coupling to a range of thermal sources in practical environments, enabling continuous macroscopic autonomous locomotion. According to our knowledge, this is the first example that transfers molecular-level changes into efficient macroscopic work output for locomotion by harvesting low-density ambient energy. Given the universality of such chemo-mechanical coupling, CoMbots with more complex structures and rotating modes, such as inhomogeneous rotation with non-constant angular velocity or acceleration, could be envisioned through rational arrangements of several CoMbots, suggesting the significant potential of our chemo-mechanical coupling to construct robust soft machineries that efficiently harvest ambient low-density energy for transferring molecular transition to macroscopic motion.

Conclusion

Inspired by the bacteria-like continuous locomotion driven by the self-sustained oscillation of their flagella through reversible coordination of highly dynamic ion binding, we developed a novel concept of self-oscillating motors, relying on dynamic Eu³⁺-pyridinediimine coordination, which enabled chemo-mechanical coupling. By integrating such dynamic coordination interactions (Eu-Pdimi, Al-Pdimi, Zr-Pdimi) into PDMS, significant temperature sensitivities to the coefficient of thermal expansion were achieved. Combining this active Eu-Pdimi-PDMS layer with a passive cellulose paper, we constructed the lanthanide-coordination motorized oscillator (CoMO), demonstrating chemo-mechanical coupling sustained oscillation with remarkable robustness (over 4000 cycles within 5 hours) with wide temperature adaptiveness (30~100 °C). Multi-modal oscillation, including reciprocal and sinusoidal motion, could also be achieved thanks to the feasibility of the mechanism. Meanwhile, through an end-to-end connection, the macroscopic oscillation was successfully amplified, achieving more efficient utilization of molecular-level transition for macroscopic motion. Furthermore, through modular assembly, CoMOs can be engineered into multimodal autonomous robots (CoMbot), proving the effectiveness of chemo-mechanical transition for supporting locomotion by harvesting ambient low-density energy.

In terms of future development, such biomimetic oscillation is achieved through the heat-triggered fast, reversible Eu³⁺ coordination with pyridinediimine-functionalized PDMS polymer. Considering the modular design of responsive polymeric materials, our chemomechanical feedback oscillating mechanism is expected to be facilely customized and expanded by utilizing diverse metal coordination interactions with similar dynamic characteristics. Other trivalent (Al³⁺) and tetravalent (Zr⁴⁺) metal ions can also be used to coordinate with Pdimi-PDMS to achieve continuous oscillations. Leveraging ion-ligand

with various dynamicity, the transition temperature of the active layer can be precisely customized, creating CoMO and CoMbots with wide temperature adaptability. This also offers opportunities for multifunctional oscillators by utilizing metal ions with unique optical, electrical, or magnetic characteristics. Similarly, the polymeric material is not restricted to Pdimi-PDMS. [50-52] It is noteworthy that stability is also indispensable for sustaining the oscillation, while dynamicity triggers the oscillation. [53,54] Thus, balancing stability and dynamicity is the merit of generating selfsustained oscillation. Our metal complex-based material provides abundant choices to achieve and regulate this coupling. [19,55,56] Within this design framework, oscillation can be further enhanced by pairing a more dynamically responsive active layer with a highly compliant passive substrate. Coupling multiple oscillators or carefully tuned resonance geometries presents additional routes to boost both amplitude and frequency, ultimately enabling CoMOs and CoMbots to perform with greater vigor, adaptability, and autonomy in harvesting ambient energy. Such dynamic bonding-enabled chemo-mechanical transducers may lead to innovations in not only more delicate chemical principles for energy harvesting and utilization but also soft locomotive robotic counterparts of living organisms, which can harvest ambient minor energy in natural settings for high-level autonomy.

Supporting Information

The authors have cited additional references within the Supporting Information.^[57-60]

Acknowledgements

T.C. and W.L. thank the support from the Natural Science Foundation of China (52473116, 22322508), Zhejiang Provincial Natural Science Foundation of China (LR23E030001).

Conflict of Interests

The authors declare no conflict of interest.

Data Availability Statement

The data that support the findings of this study are available from the corresponding author upon reasonable request.

Keywords: Ambient energy harvesting • Autonomous soft robotics • Chemo-mechanical coupling • Dynamic bonding • Self-sustained oscillation

[1] G. Li, X. Chen, F. Zhou, Y. Liang, Y. Xiao, X. Cao, Z. Zhang, M. Zhang, B. Wu, S. Yin, Y. Xu, H. Fan, Z. Chen, W. Song, W. Yang, B. Pan, J. Hou, W. Zou, S. He, X. Yang, G. Mao, Z. Jia, H. Zhou, T. Li, S. Qu, Z. Xu, Z. Huang, Y. Luo, T. Xie, J. Gu, S.

ownloaded from https

//onlinelibrary.wiley.com/doi/10.1002/anie.202518011 by University Of California, Los Angeles, Wiley Online Library on [06/11/2025]. See the Terms and Conditions (https://onlinelibrary.wiley.

and-conditions) on Wiley Online Library for rules of use; OA articles are governed by the applicable Creative Commons I

Research Article



- Zhu, W. Yang, *Nature* **2021**, *591*, 66–71, https://doi.org/10.1038/s41586-020-03153-z.
- [2] Y. Wu, J. K. Yim, J. Liang, Z. Shao, M. Qi, J. Zhong, Z. Luo, X. Yan, M. Zhang, X. Wang, R. S. Fearing, R. J. Full, L. Lin, Sci. Robot. 2019, 4, eaax1594.
- [3] W. K. Lee, D. J. Preston, M. P. Nemitz, A. Nagarkar, A. K. MacKeith, B. Gorissen, N. Vasios, V. Sanchez, K. Bertoldi, L. Mahadevan, G. M. Whitesides, Sci. Robot. 2022, 7, eabg5812.
- [4] J. Chen, F. K. Leung, M. C. A. Stuart, T. Kajitani, T. Fukushima, E. van der Giessen, B. L. Feringa, *Nat. Chem.* 2018, 10, 132–138, https://doi.org/10.1038/nchem.2887.
- [5] R. F. Shepherd, F. Ilievski, W. Choi, S. A. Morin, A. A. Stokes, A. D. Mazzeo, X. Chen, M. Wang, G. M. Whitesides, *Proc. Natl. Acad. Sci. USA* 2011, 108, 20400–20403, https://doi.org/10.1073/pnas.1116564108.
- [6] P. Zhang, I. M. Lei, G. Chen, J. Lin, X. Chen, J. Zhang, C. Cai, X. Liang, J. Liu, Nat. Commun. 2022, 13, 4775, https://doi.org/10. 1038/s41467-022-32126-1.
- [7] J. Liang, Y. Wu, J. K. Yim, H. Chen, Z. Miao, H. Liu, Y. Liu, Y. Liu, D. Wang, W. Qiu, Z. Shao, M. Zhang, X. Wang, J. Zhong, L. Lin, Sci. Robot. 2021, 6, eabe7906.
- [8] Y. Zhao, Y. Chi, Y. Hong, Y. Li, S. Yang, J. Yin, Proc. Natl. Acad. Sci. USA 2022, 119, e2200265119, https://doi.org/10.1073/pnas. 2200265119.
- [9] S. Iamsaard, S. J. Asshoff, B. Matt, T. Kudernac, J. J. Cornelissen, S. P. Fletcher, N. Katsonis, *Nat. Chem.* 2014, 6, 229–235, https://doi.org/10.1038/nchem.1859.
- [10] M. Pilz da Cunha, H. S. Kandail, J. M. J. den Toonder, A. Schenning, *Proc. Natl. Acad. Sci. USA* 2020, 117, 17571–17577, https://doi.org/10.1073/pnas.2004748117.
- [11] M. J. Ford, C. P. Ambulo, T. A. Kent, E. J. Markvicka, C. Pan, J. Malen, T. H. Ware, C. Majidi, *Proc. Natl. Acad. Sci. USA* 2019, 116, 21438–21444, https://doi.org/10.1073/pnas.1911021116.
- [12] X. Zhang, G. Chen, X. Fu, Y. Wang, Y. Zhao, Adv. Mater. 2021, 33, e2104932, https://doi.org/10.1002/adma.202104932.
- [13] C. Zhou, Y. Yang, J. Wang, Q. Wu, Z. Gu, Y. Zhou, X. Liu, Y. Yang, H. Tang, Q. Ling, L. Wang, J. Zang, *Nat. Commun.* 2021, 12, 5072, https://doi.org/10.1038/s41467-021-25386-w.
- [14] Z. Zheng, H. Wang, S. O. Demir, Q. Huang, T. Fukuda, M. Sitti, Sci. Adv. 2022, 8, eade6135, https://doi.org/10.1126/sciadv. ade6135.
- [15] J. Liu, Y. S. Huang, Y. Liu, D. Zhang, K. Koynov, H. J. Butt, S. Wu, *Nat. Chem.* 2024, *16*, 1024–1033, https://doi.org/10.1038/ s41557-024-01476-2.
- [16] W. Lu, R. Wang, M. Si, Y. Zhang, S. Wu, N. Zhu, W. Wang, T. Chen, SmartMat 2023, 5, e1190.
- [17] R. Wang, Y. Zhang, W. Lu, B. Wu, S. Wei, S. Wu, W. Wang, T. Chen, Angew. Chem. Int. Ed. 2023, 62, e202300417.
- [18] Y. S. Kim, M. Liu, Y. Ishida, Y. Ebina, M. Osada, T. Sasaki, T. Hikima, M. Takata, T. Aida, *Nat. Mater.* 2015, 14, 1002–1007, https://doi.org/10.1038/nmat4363.
- [19] B. Shin, J. Ha, M. Lee, K. Park, G. H. Park, T. H. Choi, K. J. Cho, H. Y. Kim, *Sci. Robot.* 2018, 3, eaar2629, https://doi.org/10.1126/ scirobotics.aar2629.
- [20] P. Shi, C. Chen, Z. Wang, W. Hong, S. Duan, Z. Liu, W. Hou, M. Si, C. W. Zhang, X. He, Sci. Adv. 2025, 11, eadx7189.
- [21] C. Chen, P. Shi, Z. Liu, S. Duan, M. Si, C. Zhang, Y. Du, Y. Yan, T. J. White, R. Kramer-Bottiglio, M. Sitti, T. Iwasaki, X. He, *Sci. Robot.* 2025, 10, eads1292.
- [22] Y. Zhao, Z. Liu, P. Shi, C. Chen, Y. Alsaid, Y. Yan, X. He, Nat. Mater. 2024, 24, 116–124.
- [23] X. Q. Wang, C. F. Tan, K. H. Chan, X. Lu, L. Zhu, S. W. Kim, G. W. Ho, *Nat. Commun.* 2018, 9, 3438, https://doi.org/10.1038/ s41467-018-06011-9.
- [24] R. Zheng, L. Ma, W. Feng, J. Pan, Z. Wang, Z. Chen, Y. Zhang, C. Li, P. Chen, H. K. Bisoyi, B. Li, Q. Li, Y. Lu, Adv. Funct. Mater. 33, 2023, 2301142, https://doi.org/10.1002/adfm.202301142.

- [25] A. H. Gelebart, D. J. Mulder, M. Varga, A. Konya, G. Vantomme, E. W. Meijer, R. L. B. Selinger, D. J. Broer, *Nature* 2017, 546, 632–636, https://doi.org/10.1038/nature 22987
- [26] Y. Zhao, C. Xuan, X. Qian, Y. Alsaid, M. Hua, L. Jin, X. He, Sci. Robot. 2019, 4, eaax7112.
- [27] Z. Li, N. V. Myung, Y. Yin, Sci. Robot. 2021, 6, eabi4523, https://doi.org/10.1126/scirobotics.abi4523.
- [28] Y. Hu, Q. Ji, M. Huang, L. Chang, C. Zhang, G. Wu, B. Zi, N. Bao, W. Chen, Y. Wu, *Angew. Chem. Int. Ed.* 2021, 60, 20511–20517, https://doi.org/10.1002/anie.202108058.
- [29] X. Yang, W. Shi, Z. Chen, M. Du, S. Xiao, S. Qu, C. Li, Adv. Funct. Mater. 2023, 33, 2214394, https://doi.org/10.1002/adfm. 202214394.
- [30] Z. Hu, Y. Li, J. A. Lv, Nat. Commun. 2021, 12, 3211, https://doi. org/10.1038/s41467-021-23562-6.
- [31] A. Shastri, L. M. McGregor, Y. Liu, V. Harris, H. Nan, M. Mujica, Y. Vasquez, A. Bhattacharya, Y. Ma, M. Aizenberg, O. Kuksenok, A. C. Balazs, J. Aizenberg, X. He, *Nat. Chem.* 2015, 7,447–454, https://doi.org/10.1038/nchem.2203.
- [32] F. Qi, Y. Li, Y. Hong, Y. Zhao, H. Qing, J. Yin, Proc. Natl. Acad. Sci. USA 2024, 121, e2312680121.
- [33] Y. Zhao, Q. Li, Z. Liu, Y. Alsaid, P. Shi, M. Khalid Jawed, X. He, Sci. Robot. 2023, 8, eadf4753.
- [34] J. Li, L. Mou, Z. Liu, X. Zhou, Y. Chen, Nat. Commun. 2022, 13, 5621, https://doi.org/10.1038/s41467-022-33374-x.
- [35] G. Hou, X. Zhang, F. Du, Y. Wu, X. Zhang, Z. Lei, W. Lu, F. Zhang, G. Yang, H. Wang, Z. Liu, R. Wang, Q. Ge, J. Chen, G. Meng, N. X. Fang, X. Qian, *Nat. Nanotechnol.* 2024, 19, 77–84, https://doi.org/10.1038/s41565-023-01490-4.
- [36] N. Gao, M. Li, L. Tian, A. J. Patil, B. P. Kumar, S. Mann, Nat. Chem. 2021, 13, 868–879, https://doi.org/10.1038/s41557-021-00728-9.
- [37] C. Chen, Z. Liu, P. Shi, Y. Zhao, S. Duan, Y. Du, Y. Yan, M. Si, T. Iwasaki, X. He, *Nat. Commun.* 2025, 16, 7630, https://doi.org/ 10.1038/s41467-025-62328-2.
- [38] Q. Wang, Z. Wu, J. Li, J. Wei, J. Guo, M. Yin, ACS Appl. Mater. Interfaces 2022, 14, 38972–38980, https://doi.org/10.1021/acsami. 2c11944.
- [39] Y. Zhao, Y. Hong, F. Qi, Y. Chi, H. Su, J. Yin, Adv. Mater. 2023, 35, e2207372, https://doi.org/10.1002/adma.202207372.
- [40] X. Che, T. Wang, B. Zhang, Z. Zhai, Y. Chen, D. Pei, A. Ge, M. Li, C. Li, Adv. Funct. Mater. 2024, 34, 2307830.
- [41] G. De Canio, E. Lauga, R. E. Goldstein, J. R. Soc., Interface 2017, 14, 20170491.
- [42] J. C. Deme, S. Johnson, O. Vickery, A. Aron, H. Monkhouse, T. Griffiths, R. H. James, B. C. Berks, J. W. Coulton, P. J. Stansfeld, S. M. Lea, *Nat. Microbiol.* 2020, 5, 1553–1564, https://doi.org/10.1038/s41564-020-0788-8.
- [43] S. Nakamura, T. Minamino, Biomolecules 2019, 9, 279.
- [44] S. F. Liang, C. Nie, J. Yan, Q. J. Zhang, S. Wu, Chin. J. Polym. Sci. 2021, 39, 1225–1234, https://doi.org/10.1007/s10118-021-2519-x.
- [45] J. Zhao, Z. Zhang, L. Cheng, R. Bai, D. Zhao, Y. Wang, W. Yu, X. Yan, J. Am. Chem. Soc. 2022, 144, 872–882, https://doi.org/10. 1021/jacs.1c10427.
- [46] X. Kuang, S. Wu, Q. Ze, L. Yue, Y. Jin, S. M. Montgomery, F. Yang, H. J. Qi, R. Zhao, Adv. Mater. 2021, 33, e2102113, https://doi.org/10.1002/adma.202102113.
- [47] J. C. Lai, L. Li, D. P. Wang, M. H. Zhang, S. R. Mo, X. Wang, K. Y. Zeng, C. H. Li, Q. Jiang, X. Z. You, J. L. Zuo, Nat. Commun. 2018, 9, 2725, https://doi.org/10.1038/s41467-018-05285-3.
- [48] Y.-F. Zhang, Y.-J. Ren, H.-C. Guo, S.-l. Bai, Appl. Therm. Eng. 2019, 150, 840–848, https://doi.org/10.1016/j.applthermaleng. 2019.01.029.





15213773. 0, Downloaded from https://onlinelibrary.wiley.com/doi/10.1002/anie.202518011 by University Of California, Los Angeles, Wiley Online Library on [06/11/2025]. See the Terms

conditions) on Wiley Online Library for rules of use; OA articles are governed by the applicable Creative Commons License

- [49] A. R. Manafzadeh, R. E. Kambic, S. M. Gatesy, *Proc Natl Acad Sci U S A* 2021, 118, e2023513118.
- [50] H. Zhang, H. Zeng, A. Eklund, H. Guo, A. Priimagi, O. Ikkala, Nat. Nanotechnol. 2022, 17, 1303–1310, https://doi.org/10.1038/ s41565-022-01241-x.
- [51] Y. C. Cheng, H. C. Lu, X. Lee, H. Zeng, A. Priimagi, Adv. Mater. 2020, 32, e1906233, https://doi.org/10.1002/adma.201906233.
- [52] Z. Deng, H. Zhang, A. Priimagi, H. Zeng, Adv. Mater. 2024, 36, e2209683, https://doi.org/10.1002/adma.202209683.
- [53] Y. Chen, C. Valenzuela, X. Zhang, X. Yang, L. Wang, W. Feng, Nat. Commun. 2023, 14, 3036, https://doi.org/10.1038/s41467-023-38792-z.
- [54] K. Yu, X. Ji, T. Yuan, Y. Cheng, J. Li, X. Hu, Z. Liu, X. Zhou, L. Fang, Adv. Mater. 2021, 33, e2104558, https://doi.org/10.1002/ adma.202104558.
- [55] H. Arazoe, D. Miyajima, K. Akaike, F. Araoka, E. Sato, T. Hikima, M. Kawamoto, T. Aida, *Nat. Mater.* 2016, 15, 1084–1089, https://doi.org/10.1038/nmat4693.

- [56] C. H. Li, C. Wang, C. Keplinger, J. L. Zuo, L. Jin, Y. Sun, P. Zheng, Y. Cao, F. Lissel, C. Linder, X. Z. You, Z. Bao, *Nat. Chem.* 2016, 8, 618–624, https://doi.org/10.1038/nchem.2492.
- [57] B. Zhan, S. Wei, Z. Hu, H. Liu, H. Qiu, Q. Liu, W. Lu, T. Chen, Macromol. Mater. Eng. 2021, 306.
- [58] I. D. Brown, Chem. Rev. 2009, 109, 6858–6919, https://doi.org/10. 1021/cr900053k.
- [59] N. E. Brese, M. O'Keeffe, Acta Crystallogr. B Struct. Science 1991, 47, 192–197, https://doi.org/10.1107/S0108768190011041.
- [60] I. D. Brown, Accumulated table of bond valence parameters, https://www.iucr.org/resources/data/datasets/bond-valence-parameters.

Manuscript received: August 15, 2025 Revised manuscript received: September 26, 2025 Manuscript accepted: October 23, 2025

Version of record online: ■■, ■